Investigations in the sheath region of a radio frequency biased inductively coupled discharge

E. C. Benck, A. Schwabedissen, A. Gates,[a] and J. R. Roberts[b]
National Institute of Standards and Technology, Gaithersburg, Maryland 20899

(Received 10 April 1997; accepted 11 August 1997)

Temporally and spatially resolved optical emission, as well as Langmuir and electric probe measurements, were used to investigate the effects of radio frequency (rf) biasing near an electrode in an inductively coupled plasma cell. The plasma source is a modification of the Gaseous Electronics Conference rf Reference Cell. Emission from the atomic argon 750.387 nm transition was observed. With the lower electrode grounded, the optical emission did not exhibit any rf modulations. However, for a constant rf bias power of 9 W at frequencies from 1.695 to 33.9 MHz applied to the lower electrode, various waveforms were observed in the temporal evolution of the optical emission near the electrode as well as in the bulk plasma. Also, for pressures between 0.67 and 13.3 Pa of argon and a rf power of 9 W at a frequency of 2.712 MHz, the oscillations in the optical emission near the biased electrode showed the presheath/sheath region rapidly shrinking with increasing pressure. The dc sheath voltage drop, determined from Langmuir and electric probe measurements, did not exhibit a dependence on the applied rf frequency, but varied nearly linearly with the ratio of the bias power to the power dissipated in the plasma. [S0734-2101(98)00301-7]

I. INTRODUCTION

The future requirement to achieve high throughput and yield for the fabrication of semiconductor devices with critical dimensions $< 0.25\ \mu$m will require plasma processing tools delivering high plasma densities and controllable ion energy distributions at low pressures. These characteristics are essential to achieve highly anisotropic features, etch selectivity and minimize substrate damage. This limits the use of capacitively coupled discharges because it is not possible to simultaneously attain low ion impact energies and high plasma densities at sufficiently low pressures. The development of high plasma density ($> 1\times10^{11}$ cm^{-3}), low pressure (< 10 Pa) sources has been accomplished with the use of electron cyclotron resonance (ECR), helicon waves and planar inductively coupled plasmas (ICPs).[1–8]

We will describe experimental observations of the temporally and spatially resolved optical emission in the presheath/sheath plasma region, as well as electric and Langmuir probe measurements in a planar ICP source with an independently biased lower electrode. The variation of the input power to the inductor coil demonstrates the possible independent control of ion flux and the radio frequency (rf) biasing of the lower electrode illustrates control of the ion energy to the substrate surface.

The temporally and spatially resolved optical emission measurements were made in the presheath/sheath region near the lower electrode in the ICP. These measurements were done by applying a variable rf voltage at various frequencies to the lower electrode. The sheath was estimated to be smaller than our optical resolution, so only the presheath region is resolved in our measurements.

A Langmuir probe was used to measure the dc component of the plasma potential of the bulk plasma. Since the dc plasma potential is related to the energy that the ions gain in the sheath region, this can be used with additional electrical measurements to determine the mean energy of ions impinging on the lower electrode. The ion energy distribution (IEDF) of a planar ICP source with grounded lower electrode has been measured by Hopwood,[9] Kortshagen and Zethoff,[10] and for an ICP identical to our ICP source by Woodworth and co-workers.[2] In pure argon, rather simple IEDFs were observed, with just one relatively narrow profile, the peak of which is well separated from zero energy. The mean energy of this IEDF was nearly equal to the plasma potential in the bulk plasma with typical values between 20 and 30 eV which increased with decreasing pressure. The simple structure of the IEDF in this ICP compared to a capacitively coupled discharge is due to the lower pressure in ICPs and the small sheath thickness which results in a fast sheath transition time with no collisions. IEDF measurements with the ion energy analyzer beneath a biased lower electrode are difficult and have not yet been reported for a planar ICP.

II. EXPERIMENTAL APPARATUS

A. Inductively coupled cell description

The ICP cell used as the plasma source in these experiments is a modified Gaseous Electronics Conference (GEC) rf Reference Cell[11,12] (see Fig. 1). The cylindrical vacuum chamber is constructed of stainless steel with eight radial copper-gasketed flanges centered at the chamber midplane. Two of them are 203 mm diam flanges fitted with 136 mm diam quartz windows for optical emission spectroscopy

[a]Permanent address: Miami University, Oxford, Ohio 45056.
[b]Electronic mail: james.roberts@nist.gov

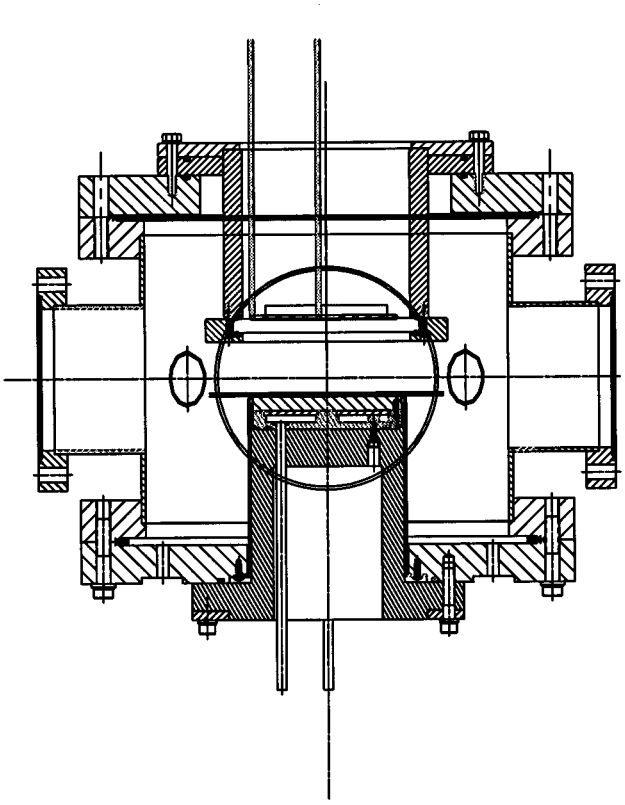

FIG. 1. Cross sectional diagram of the ICP cell. The large circle at the center of the diagram represents the position of TROES viewport.

(OES) observations. This allows the emission from the discharge to be observed throughout the ultraviolet, visible and infrared regions of the spectrum.

The power was induced into the chamber by a five-turn planar coil based on the design of Miller *et al.*[13] The coil is 100 mm in outer diameter, 1.3 μH in inductance, and is made of 3 mm diam copper tubing. It is held rigidly in place and is electrostatically shielded from the plasma by a radially spoked patterned brass foil.[14] The coil is separated from the plasma by a 10-mm-thick quartz vacuum plate, an electrostatic shield, and a 3-mm-thick quartz insulator. The spacing between the quartz vacuum interface and the lower electrode is 41 mm. The lower electrode is a 3 mm thick, 160 mm diam stainless steel plate which can be biased by a variable frequency signal generator and a rf power amplifier.

The gas is introduced into the chamber through one of four, 70 mm diam ports, 45° to the OES ports. The pressure and flow rate are maintained by a variable conductance valve and the turbomolecular pump speed. The other three 70 mm flanges are used to mount pressure transducers, probes, etc. Two additional ports, orthogonal to the OES ports, are 150 mm diam flanges to accommodate the turbomolecular pump, ion energy mass spectrometry probes, electric probes, and Langmuir probes.

The coil voltage is measured by a capacitive voltage probe, calibrated (without plasma) with reference to a commercial resistive voltage probe. The coil current is monitored at the outer, grounded lead by an inductively coupled probe, also calibrated with reference to a commercial current probe. A matching network is employed with the coil and consists of two variable air-dielectric capacitors and several fixed capacitors. They are connected directly to the coil to minimize resistive losses.[13] The variable capacitors were adjusted for minimum reflected power for each plasma condition by monitoring with a rf power meter. Data were taken with respect to the plasma power, the power dissipated in the plasma, P_{dis}, rather than the total input power. This was done since the total input power may depend on external parameters, such as the characteristics of the induction coil, matching circuit, and transmission line. The value of P_{dis} is obtained from a measurement of the total power from the supply by a power meter, P_{input}, minus the I^2R_{eff} power loss in the coil,[13,15] i.e., $P_{\text{dis}}=P_{\text{input}}-I^2R_{\text{eff}}$.

The lower electrode was biased with frequencies ranging from 1.695–33.9 MHz using a rf signal generator and a rf power amplifier. For frequencies below 20 MHz, a blocking capacitor was inserted between the power amplifier and the lower electrode which allows a dc self-bias to develop on the electrode. Commercial voltage and current probes were located at the power leads to the lower electrode. The value of the bias power dissipated in the plasma is calculated by means of a circuit parameter model[16] and the measured voltage, current, and phase of the rf power applied to the electrode leads. For all experiments, the bias frequencies used were only multiples and fractional multiples of 13.56 MHz because of restrictions within the electrical circuit model. As the frequency increased, while maintaining a constant power dissipation into the plasma, the amount of reflected power from the cell rapidly increased. Therefore, the blocking capacitor was replaced with a matching network to minimize the reflected power for frequencies above 20 MHz. If the matching network was not utilized, the voltage waveform became strongly perturbed with odd harmonics (between $\sim$ 90 and 100 MHz) of the fundamental bias frequency. When this occurred, the plasma seemed to occupy the entire vacuum chamber and created a large amount of rf electrical noise in the time-resolved optical emission spectroscopy (TROES) detection apparatus.

B. Optical emission spectroscopy

The light collection optics, monochromator, and data recording systems used for the OES are schematically represented in Fig. 2 and are described in a previous reference.[17] Mirrors M2 and M3 form a periscope which is used to vertically scan the observation region within the plasma. The entire optical apparatus is mounted on a movable table which allows for horizontal scanning of the plasma emissions. The focusing mirror M4 creates a 1:2 image of the 50 μm spectrometer entrance slit in the plasma. The periscope rotates the image of the slit so that its long dimension is parallel to the biased electrode. The vertical spatial resolution was controlled by the apertures. Two types of apertures where used:

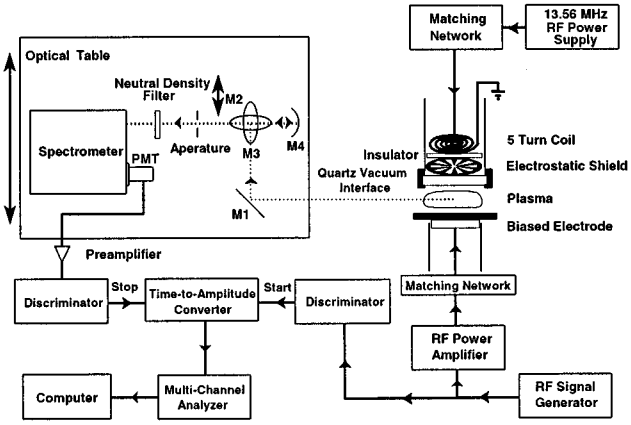

FIG. 2. Schematic diagram of experimental layout for time-resolved optical emission spectroscopic measurements. M1, M2, M3, and M4 are mirrors. PMT is a cooled photomultiplier tube for photon counting.

a circular 3.6 mm aperture with a vertical spatial resolution of ± 0.4 mm and 1-mm-wide slit with a vertical spatial resolution of ± 0.2 mm.

Time-averaged OES measurements were made with a picoammeter to measure the average photomultiplier current. The picoammeter integrates the current for ~ 0.1 s, averaging out any rf fluctuations in the optical emission. Each time-averaged data point presented in this article represents the average of five consecutive measurements with the error bars determined by the standard deviation of the measurements.

TROES measurements were performed using a time-to-amplitude converter (TAC) and a multichannel analyzer (MCA). The start pulse for the TAC is triggered from the rf signal generator used to bias the lower electrode. The TAC stop pulse is generated by the next photon arriving at the photomultiplier from the plasma. The output of the TAC is accumulated in a MCA. The resulting signal is therefore, the distribution of delay times for the arrival of the next photon. This is equivalent to the time-resolved optical emission distribution as long as the average number of photons is $<< 1$ during the time interval being examined. Typically, data from more than 3 M photons were collected for each waveform and required from 10 min to over an hour of data acquisition, depending on the light intensity and the bias frequency.

The $4s'[1/2]_1^0 - 4p'[1/2]_0$ transition in Ar I with a wavelength of 750.387 nm (Ref. 18) and a natural lifetime of 21 ns was used in both the time-averaged and time-resolved OES measurements. The electron excitation energy of the upper state from the ground state is 13.48 eV. For the typical densities and electron temperatures in this ICP plasma,[15] the electron excitation rate from metastable states calculated from excitation cross sections[19] is several orders of magnitude less than the direct excitation from the ground state. Therefore, assuming that the neutral gas density is spatially uniform, the OES monitors the changes in the density of electrons with energies > 13.48 eV. In the bulk plasma the plasma potential should not significantly vary with distance from the biased electrode over the narrow observation region of < 2 mm. As a result, due to the nonlocal nature of the electron energy distribution function (EEDF) in this type of ICP[1,13,20] there should not be a significant change in the EEDF as a function of position, and therefore, changes in the high energy electron density should be indicative of what is occuring to the total electron density. In the presheath region this may no longer hold since there is a potential drop of $\sim T_e/2$ (Ref. 21) which may alter the EEDF. Because of the narrow width of the sheath, stochastic heating of electrons in the sheath is not significant.[3]

C. Langmuir and electric probe description

A commercial Langmuir probe assembly was attached to a manually operated $x-y-z$ manipulator and is mounted to one of the 70 mm flanges of the cell chamber. The dc component of the plasma potential, V_{pl}, in the bulk plasma was measured with a cylindrical probe with a tip radius of 190 μm and a tip length of 6 mm.

The compensation of a Langmuir probe for the rf fluctuations of the plasma potential is critical for capacitively coupled rf discharges.[22,23] In this type of discharge the plasma potential as well as the voltage drop in the probe space-charge sheath are modulated with amplitudes of typically tens of volts. The rf plasma potential oscillations in ICPs with a grounded lower electrode are much smaller than in capacitive rf discharges. They should be zero in a perfectly electrostatically shielded ICP. In our Langmuir probe the rf currents are sufficiently suppressed when the lower electrode is biased between 2.712 and 33.9 MHz by two series inductors, and an additional metallic cylinder to allow unambiguous probe characteristics to be interpreted in this frequency band. The cylinder is capacitively connected to the probe and is in front of the inductors in order to reduce the capacitive impedance between the probe tip and the plasma.

A wire loop probe[16,24] was used to monitor the peak-to-peak rf amplitude of the plasma potential. Values < 2 V at 13.56 MHz were measured for most operating conditions in the case where the lower electrode was not biased. This finite amplitude is due to the residual capacitive coupling from the coil to the plasma. With a rf biased lower electrode, however, the rf amplitudes of the plasma potential are larger and grow with applied power to amplitudes ~ 8 V at $P_{\mathrm{bias}} = 9$ W, since the discharge is now both capacitively and inductively driven.

Whether the compensation of the probe is sufficient to determine the plasma potential can be determined by observing the second derivative of the probe characteristic $I''(U_{\mathrm{pr}})$, where U_{pr} is the voltage applied to the probe. Ideally, when the probe potential is varied at values around the plasma potential, $I''(U_{\mathrm{pr}})$ should have a single maximum and a single minimum close to each other.[25] The dc component of the plasma potential is calculated from the zero crossing of the second derivative. We observed second derivatives with a single maximum and a single minimum for bias frequencies, f_{bias}, between 2.712 and 33.9 MHz (see Fig. 3), while

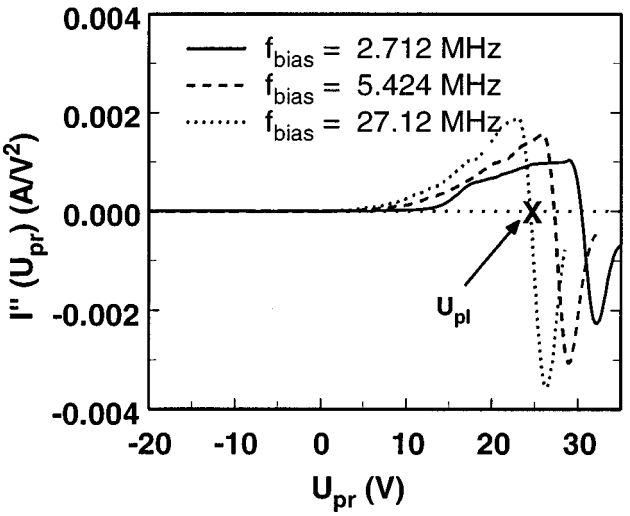

FIG. 3. Second derivatives of the current–voltage probe characteristics at different bias frequencies (P_{bias} =9 W, P_{dis}=165 W).

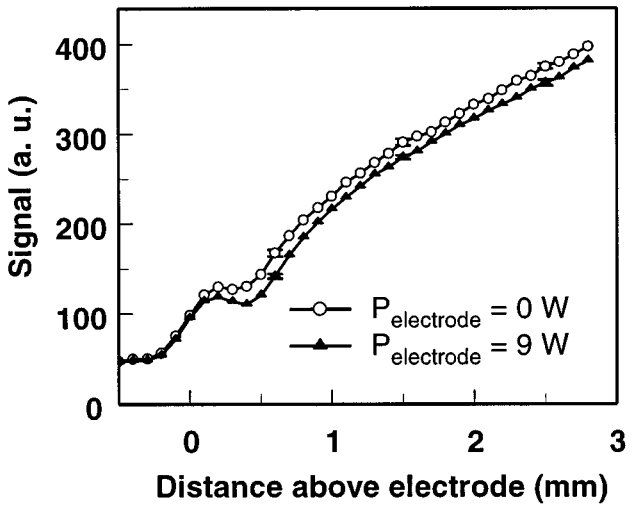

FIG. 4. Time-averaged line-of-sight optical emission of the Ar I 750.387 nm transition vs distance above the electrode for a biased (f_{bias}=2.712 MHz) and grounded lower electrode at p=1.33 Pa and P_{dis}=56 W. The signal does not go to zero for negative distances due to reflected light off the electrode surface. The error bars indicate the standard deviation of the measurements.

at f_{bias} = 1.695 MHz the second derivative showed several maxima and minima. This indicates that the probe is insufficiently frequency compensated.[25] Under these circumstances the determination of the plasma potential from the zero crossing of $I''(U_{pr})$ can lead to false results. Hence, we only present results for V_{pl} with f_{bias} between 2.712 and 33.9 MHz.

III. EXPERIMENTAL RESULTS

A. Time-averaged and time-resolved optical emission spectroscopy

The line-of-sight, time-averaged optical emission near the lower electrode for the grounded and biased cases is shown in Fig. 4. The intensity of the optical emission rapidly increases with distance from the electrode. The small maximum at the electrode edge is caused by a reflection from the corner of the electrode. Biasing the electrode decreases the optical emission throughout the plasma. In order to more easily identify the presheath/sheath region of the plasma, the percent normalized difference of the optical emission with and without a biased electrode is shown in Fig. 5 for two bias frequencies. As can be seen from Fig. 5, a region of decreased optical emission extends ~1 mm from the electrode surface. The sheath width, based on the Child–Langmuir law and other theoretical models[24,26] in these types of discharges is typically only 0.2 mm. Since this is smaller than the spatial resolution of the optical system, the sheath region observed is part of the presheath. In the presheath the ions begin to be accelerated toward the electrode, but the ion velocities are still low enough so that quasineutrality can be maintained. The physical dimension of the presheath is determined by such processes as electron-ion collisions, ion-neutral collisions, and geometric factors.[27] As the ions are accelerated, the ion density must decrease, and due to quasineutrality, the electron density also decreases, resulting in the observed decrease in the optical emission. Similarly, the suppression of optical emission in the bulk plasma is an indication that the electron density has decreased throughout the plasma. Biasing with rf at 2.712 and 27.12 MHz and constant power

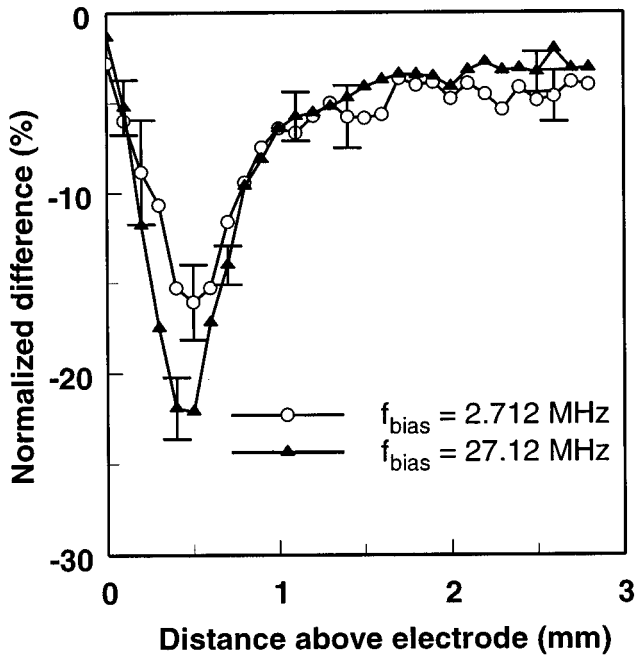

FIG. 5. Normalized difference in percent ($Sig_{P=9}-Sig_{P=0}$)/$Sig_{P=0}\times 100$) of the time-averaged optical emission with (P_{bias}=9 W) and without (P_{bias}=0 W) a biased electrode versus distance above the electrode at p=1.33 Pa and P_{dis}=56 W for two bias frequencies. Each error bar is based on the propagated standard deviation of the original optical emission measurements.

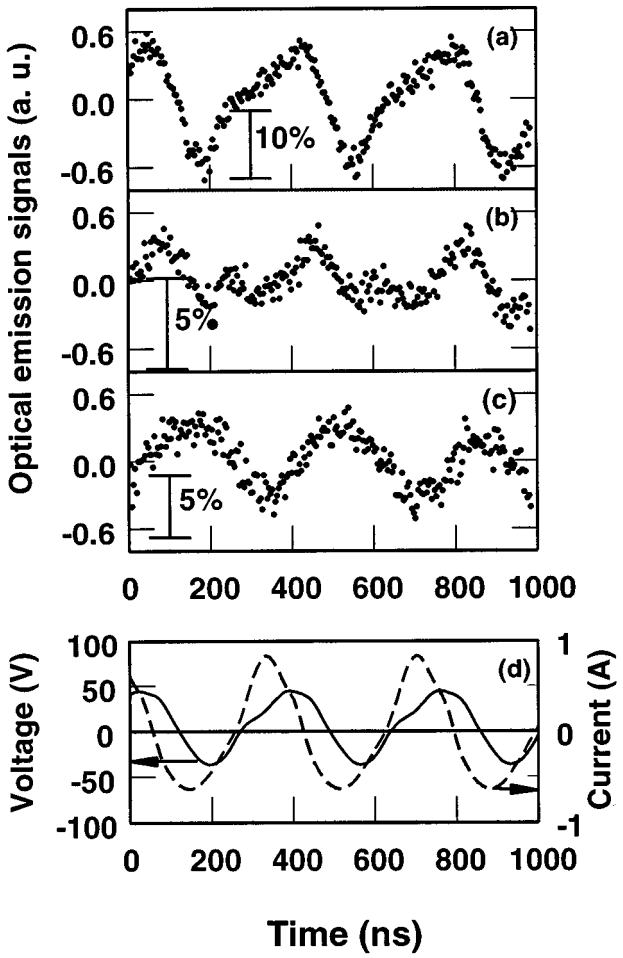

FIG. 6. TROES vs time for f_{bias}=2.712 MHz at a distance of (a) 0.5, (b) 0.7, and (c) 1.1 mm above the electrode surface, and (d) the corresponding voltage and current waveforms at the electrode surface at p=1.33 Pa, P_{dis}=56 W and P_{bias}=9 W. The marked vertical percent scales indicate the corresponding percentage of the time-averaged (dc) signal, which has been subtracted from the original data.

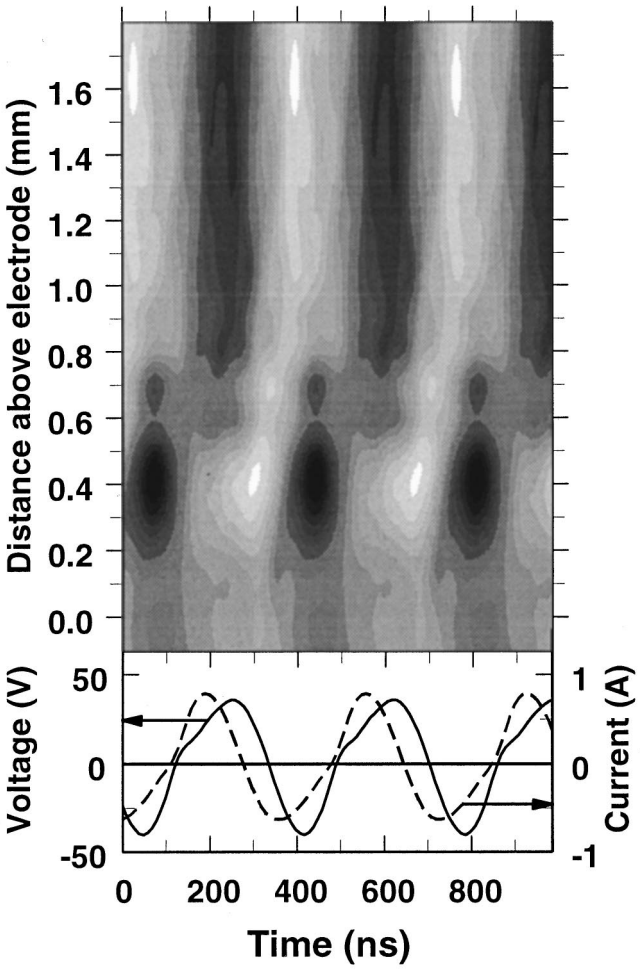

FIG. 7. Contour plot of TROES vs time and distance above the lower electrode for f_{bias} =2.712 MHz at p=1.33 Pa, P_{dis}=56 W and P_{bias}=9 W. The corresponding voltage and current waveforms at the electrode surface are presented below the contour plot. The vertical spatial resolution is ±0.2 mm.

input, yielded similar spatial dimensions for the presheath, indicating that the presheath width does not significantly depend on the bias frequency (see Fig. 5).

The TROES measurements were made with an input power of 9 W into the plasma from the lower electrode. At this power level the plasma source could be operated for long periods (many hours) without significant sputtering of metal onto the quartz vacuum interface. The amplitude of rf oscillations in the TROES was typically $<$ 10% of the time-averaged signal. In the graphical presentation of the TROES data, the time-averaged component has been subtracted to emphasize optical emission oscillations, which correlate with the electron density oscillations.

Three different types of behavior could be observed as a function of the bias frequency. First, at low bias frequencies between 1.695 and 5.424 MHz, as seen in Fig. 6, the oscillations in the plasma were relatively large in both the bulk and presheath regions. There exists a significant phase shift in the waveforms between the bulk and presheath regions. This phase shift is particularly noticeable in the contour plot of the TROES oscillations shown in Fig. 7. The TROES data for Fig. 7 was taken with the ± 0.2 mm spatial resolution at 0.1 mm intervals near the electrode, and at 0.2 mm intervals further into the bulk plasma. A sine wave expansion, including the fundamental and the next four higher harmonics, has been fitted to the data after which the dc component has been subtracted. Black shading and white shading on Fig. 7 correspond to the regions of minimum and maximum signals, respectively. The TROES waveform in the presheath (z ≈ 0.4 mm) closely follows the voltage waveform applied to the lower electrode. In the bulk plasma, the TROES waveform seems more closely related to the inverse of the current waveform, i.e., the maximum of the current occurs at approximately the same time as the minimum of the TROES signal.

Second, Fig. 8 shows typical TROES behavior at intermediate frequencies between 5.424 and 20.34 MHz. The TROES oscillation amplitudes are greatly reduced, especially in the bulk plasma. In some cases no bulk oscillations

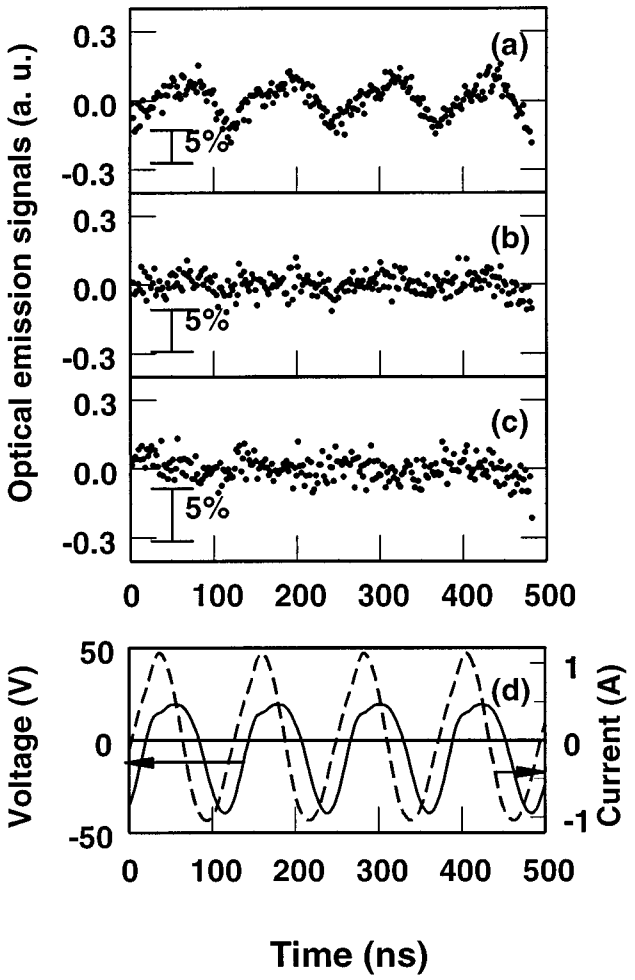

FIG. 8. TROES vs time for f_{bias} = 8.136 MHz at a distance of (a) 0.5, (b) 0.7, and (c) 1.1 mm above the electrode surface, and (d) the corresponding voltage and current waveforms at the electrode surface at p = 1.33 Pa, P_{dis} =56 W and P_{bias}=9 W. The marked vertical percent scales indicate the corresponding percentage of the time-averaged (dc) signal, which has been subtracted from the original data.

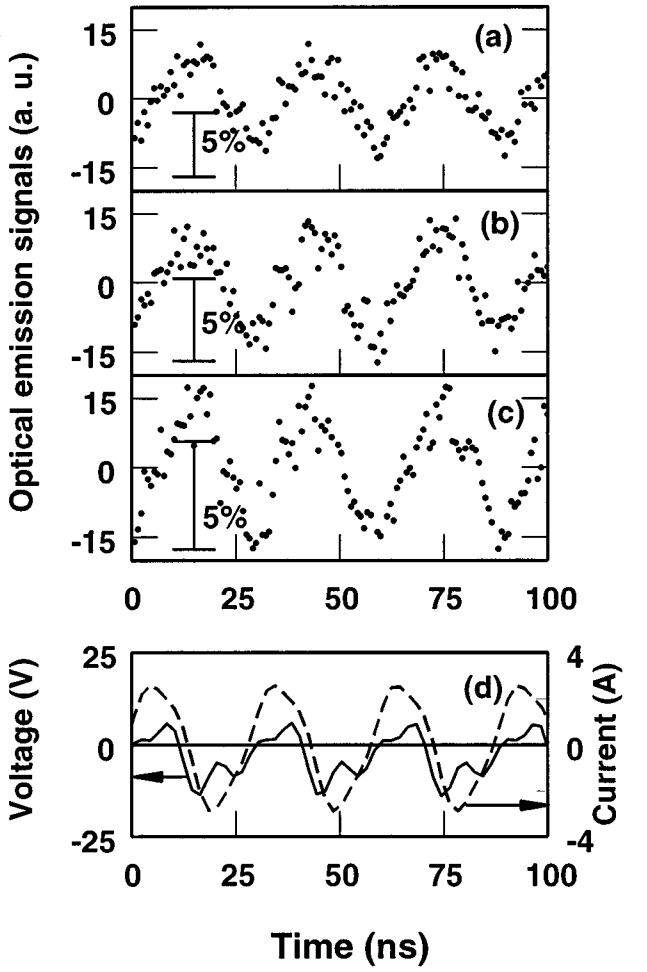

FIG. 9. TROES vs time for f_{bias}=33.9 MHz at a distance of 0.5 (a), 0.7 (b), 1.1 mm (c) above the electrode surface and the corresponding voltage and current waveforms at the electrode surface, and (d) at p=1.33 Pa, P_{dis}= 56 W and P_{bias}=9 W. The marked vertical percent scales indicate the corresponding percentage of the time-averaged (dc) signal, which has been subtracted from the original data.

were observed above our noise levels. Because of the very low signal intensities in this region, accurate measurements of the phase shifts between the bulk and presheath were not possible.

Third, at higher frequencies between 22.6 and 33.9 MHz, the TROES behavior began to change slightly, as shown in Fig 9. The amplitude of the oscillations in the bulk plasma have begun to increase. In this region, there is no phase shift between the bulk and presheath regions of the plasma. There exists a systematic uncertainty of ~10 ns between the timing of the TROES and electrical waveforms.

Figures 10–13, show the effects of changing pressure on the TROES signal. In Figs. 10–13, the corresponding voltage and current waveforms at the electrode surface are presented below the contour plot. The TROES data for Figs. 10–13 were taken with a vertical spatial resolution of ± 0.4 at 0.1 mm intervals near the electrode and at 0.2 mm intervals further into the bulk plasma. Similar to Fig. 7, the data were fitted to a sine wave expansion and the dc component was subtracted. The same, equally spaced gray scale contours were used on Figs. 10–13 to represent the relative intensify of the TROES data. Pressures from 0.67 to 13.3 Pa were chosen to cover the transition from a collisionless to collisional plasma.[28,29] The rf power supplied to the coil was maintained at 100 W. The plasma densities measured with the Langmuir probe varied from 5×10^{10} cm^{-3} to an estimated 8×10^{11} cm^{-3}. The lower electrode was biased at a frequency of 2.712 MHz with a constant power of 9 W. Under these conditions the voltage across the sheath, determined from Langmuir probe and electrical data, decreased from 39 to 30 V as the pressure increased from 0.67 to 2.66 Pa. The sheath voltage for 13.3 Pa could not be determined since the plasma density was too high to operate the Langmuir probe.

The TROES data represented in Figs. 10–13 clearly shows that the width of the presheath shrinks with increasing pressure. In addition, the oscillations in the bulk for 13.3 Pa

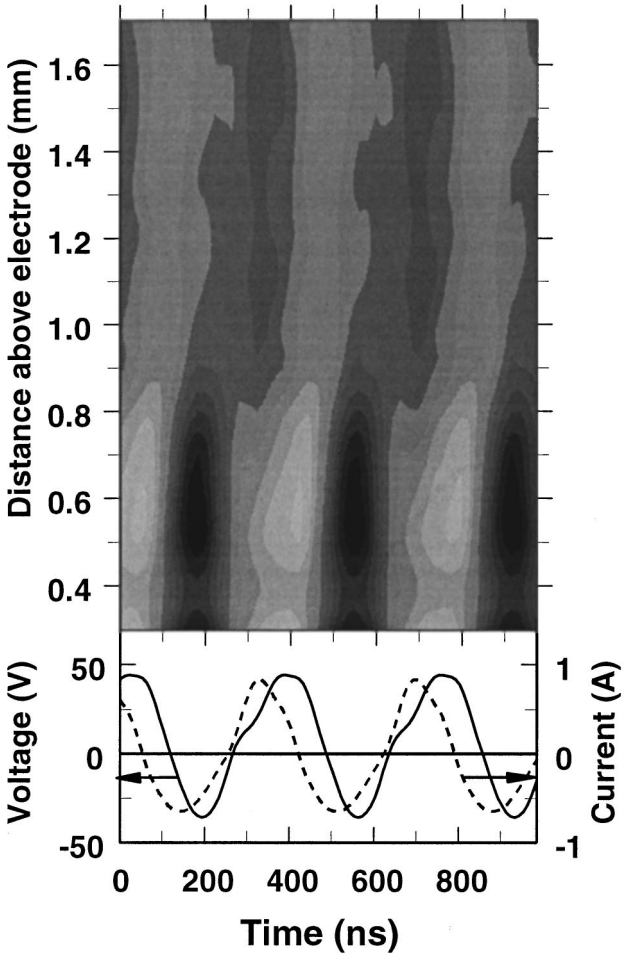

FIG. 10. Contour plot of TROES vs time and distance above the lower electrode at $p=0.67$ Pa, for $P_{\text{dis}}=54$ W, $f_{\text{bias}}=2.712$ MHz. $P_{\text{bias}}=9$ W and $N_e=5.1\times10^{10}$ cm^{-3}.

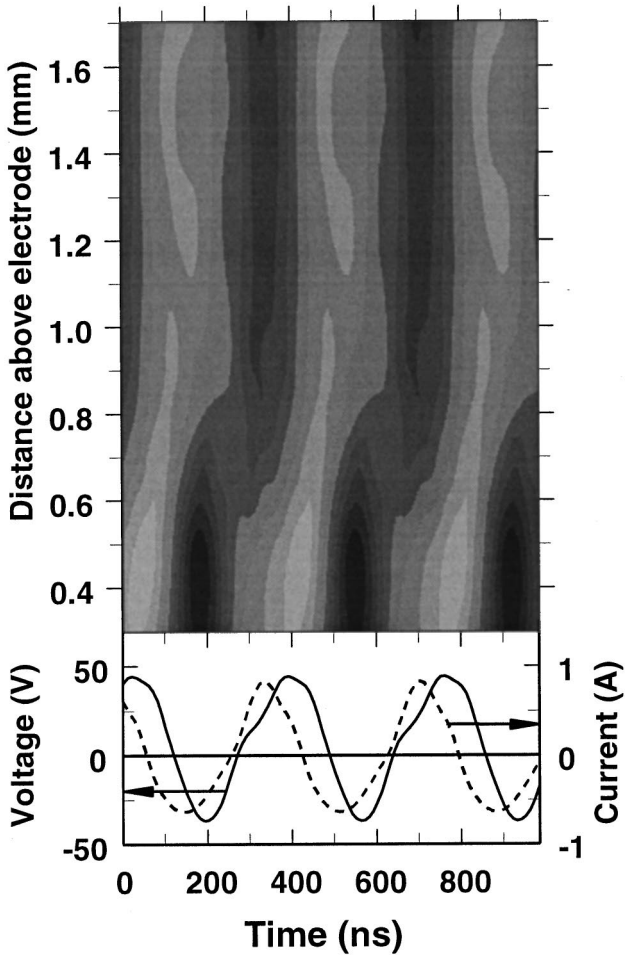

FIG. 11. Contour plot of TROES vs time and distance above the lower electrode at $p=1.33$ Pa, for $P_{\text{dis}}=56$ W, $f_{\text{bias}}=2.712$ MHz, $P_{\text{bias}}=9$ W, and $N_e=8.5\times10^{10}$cm^{-3}.

continue to grow with increasing distance from the lower electrode and the maxima become much more sharply peaked than the minima.

B. Electrical and Langmuir probe measurements

The Langmuir probe measurements were performed at bias powers ranging from 2.4–20 W and at coil input powers ranging from 100 to 350 W (corresponding to plasma powers, P_{dis}, between 60 and 240 W). The argon gas pressure was kept constant at 1.33 Pa at a flow rate of 3.7 μmol/s. All measurements were performed on the cylindrical discharge axis, 6 mm above the lower electrode. With no bias applied to the lower electrode, the plasma potential, V_{pl}, is 22 ± 1 V and does not vary with plasma power.

When the lower electrode was biased at various frequencies and a constant power of 9 W, we observed an increase of the bulk plasma potential compared to the nonbias case [see Fig. 14(a)]. In the biased case, the highest plasma potential was 36 V at 2.712 MHz and the smallest potential was 24 V at 20.34 MHz. Simultaneously, from electrical measurements, we observed a similar behavior in the dc bias of the lower electrode, $V_{\text{dc bias}}$, as a function of the applied frequency [see Fig. 14(a)]. The difference between the plasma potential and the dc bias voltage of the lower electrode determines the dc sheath voltage drop V_{sh} ($V_{\text{sh}}=V_{\text{pl}}-V_{\text{dc bias}}$). A plot of V_{sh} vs f_{bias} in Fig. 14(b) demonstrates that the dc sheath voltage drop does not depend upon the applied bias frequency within the experimental error. The voltage across the sheath did vary slowly with the condition of the electrode surface. After extensive cell operation (>50 h) V_{sh} was $\sim$30 V.

Another result was observed at a constant rf bias frequency, $f_{\text{bias}} = 2.712$ MHz, when both the bias power and the power dissipated in the plasma were varied. We found that the plasma potential, V_{pl}, increases nearly linearly as the ratio of the rf bias power to the power dissipated in the plasma, $P_{\text{bias}}/P_{\text{dis}}$, increased. Also observed as a function of this ratio was that $V_{\text{dc bias}}$ remained nearly constant. Since the dc sheath voltage drop, V_{sh}, is the difference between V_{pl} and $V_{\text{dc bias}}$, this result indicates that V_{sh} varies linearly with the ratio $P_{\text{bias}}/P_{\text{dis}}$. This can be seen in Fig. 15.

A feature of this ICP with biased lower electrode is the change of the phase ϕ between the ac component of the rf current and voltage [see Fig. 16(a)] as the bias frequency is

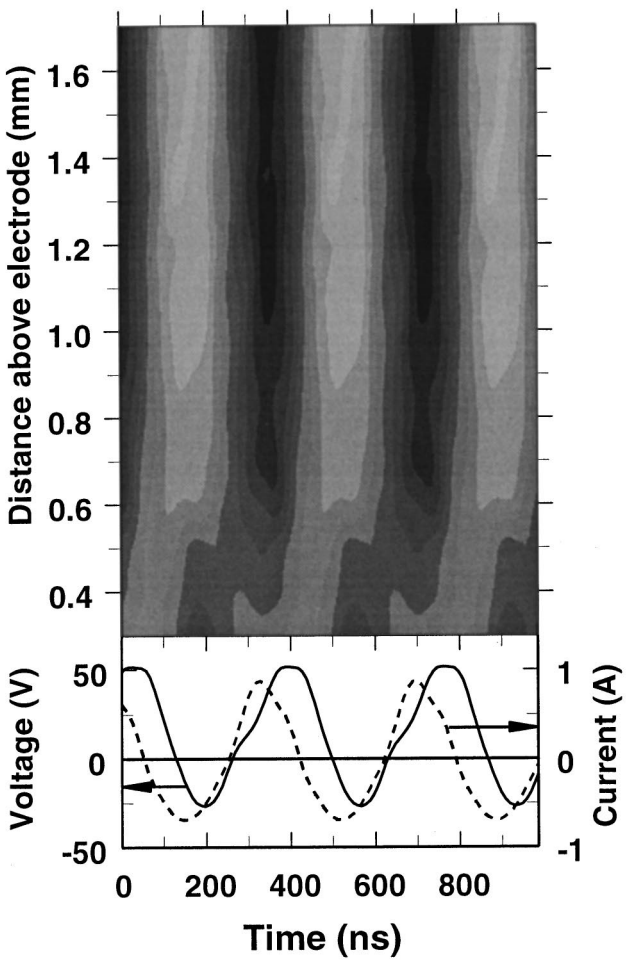

FIG. 12. Contour plot of TROES vs time and distance above the lower electrode at $p=2.66$ Pa, for $P_{\text{dis}}=62$ W, $f_{\text{bias}}=2.712$ MHz, $P_{\text{bias}}=9$ W and $N_e=1.2\times10^{11}$ cm^{-3}.

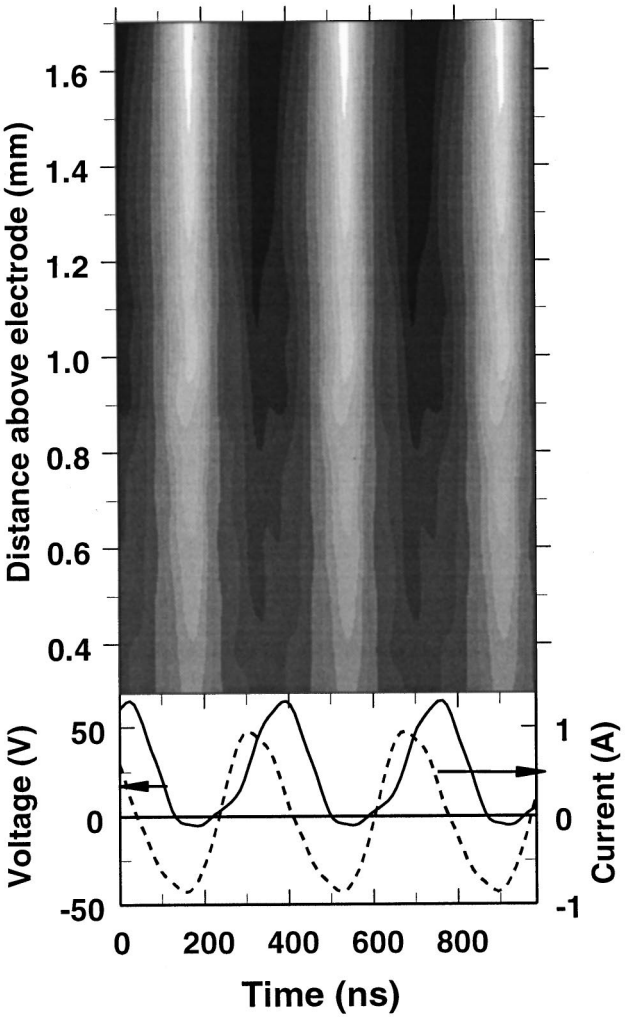

FIG. 13. Contour plot of TROES vs time and distance above the lower electrode at $p=13.3$ Pa, for $P_{\text{dis}}=71$ W, $f_{\text{bias}}=2.712$ MHz , and $P_{\text{bias}}=9$ W. The electron density was estimated to be $N_e=8\times10^{11}$ cm^{-3} in the unbiased plasma.

varied. As can be seen in Fig. 16(b), the plasma-bias electrode system becomes highly inductive at frequencies above 25 MHz, resistive near 10 MHz and more capacitive for frequencies below 10 MHz.

IV. DISCUSSION

Plasma parameters adjacent to the lower electrode determine much of the behavior of the sheath. Magnetic fields from the coil in this region are low enough to treat this as an unmagnetized plasma.[30] Because the Langmuir probe could not reach any closer than 5 mm from the electrode surface, a linear fit to the available Langmuir probe data was used to estimate the conditions adjacent to the electrode. The electron density and temperature adjacent to the electrode are estimated to be 6×10^{10} cm^{-3} and 4 eV, respectively, in an unbiased plasma with a pressure of 1.33 Pa and $P_{\text{dis}}=56$ W. This results in an ion plasma frequency, Ω_p, of $\sim$8 MHz near the surface, where $\Omega_p=(4\pi n_{\text{ion}}e^2/M_{\text{ion}})^{1/2}$, n_{ion} is the number of ions and M_{ion} is the ion mass. The production of ion plasma waves are often associated with the perturbation of the plasma from a biased electrode.[31] Typically, for bias frequencies $f_{\text{bias}}>>\Omega_p$ the ions respond only to the time-averaged potential within the sheath and for $f_{\text{bias}}<<\Omega_p$ the ion motion is influenced by the rf fields. For bias frequencies $f_{\text{bias}}\sim\Omega_p$, the expected behavior is less clear. The ion temperature in the ICP is on the order of 0.3 eV.[32] Therefore, instead of a sharp cutoff frequency for ion plasma waves which would be expected in the limit as $T_i\rightarrow0$, there will only be a reduction of the ion plasma wave phase velocity occurring around the ion plasma frequency. Although plasma waves with frequencies above the ion plasma frequency are possible, their influence on the plasma is significantly reduced by Landau damping which increases with increasing frequency.[33] The Landau damping coefficient can increase exponentially as the frequency approaches the ion plasma frequency.[34] Therefore, the amplitude of the ion plasma waves in the discharge should show a sharp decrease as frequencies approach the ion plasma frequency.

In the low frequency region from 1.695 to 5.424 MHz, the bias frequency is below the ion plasma frequency ($f_{\text{bias}}<<\Omega_p$), and therefore, the velocity of ions traversing the

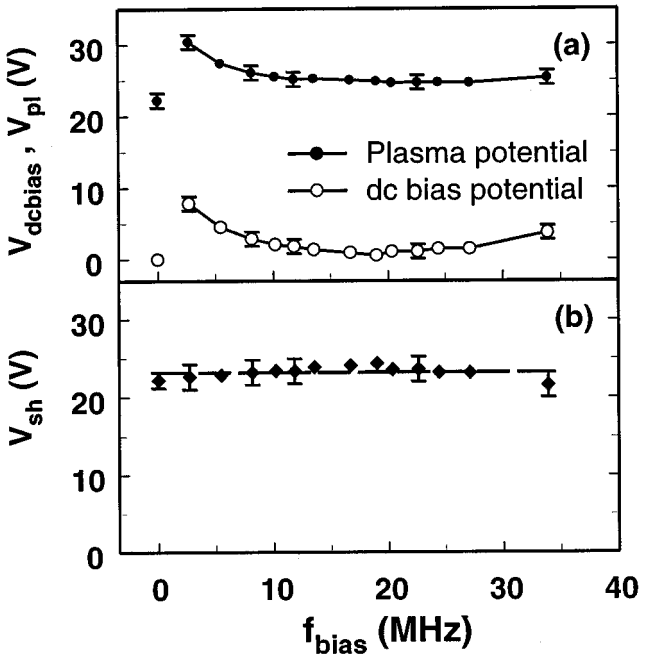

FIG. 14. (a) Plasma potential and dc component of the voltage to the lower electrode and (b) the dc sheath voltage drop for different bias frequencies (P_{bias}=9 W, P_{dis}=165 W). The dashed (- - - -) line is a linear least squares fit to the data.

presheath will be modulated by the bias rf fields. When the voltage on the electrode is at a maximum, the ion velocity slows causing an increase in the ion density. Because of quasineutrality at this position in the plasma, the electron density will also increase, producing a maxima in the TROES signal. This implies that the flux of ions reaching the sheath is not uniform in time, and therefore should influence the IEDF at the electrode surface. In the bulk plasma, the electron density modulations are being controlled by the ac-

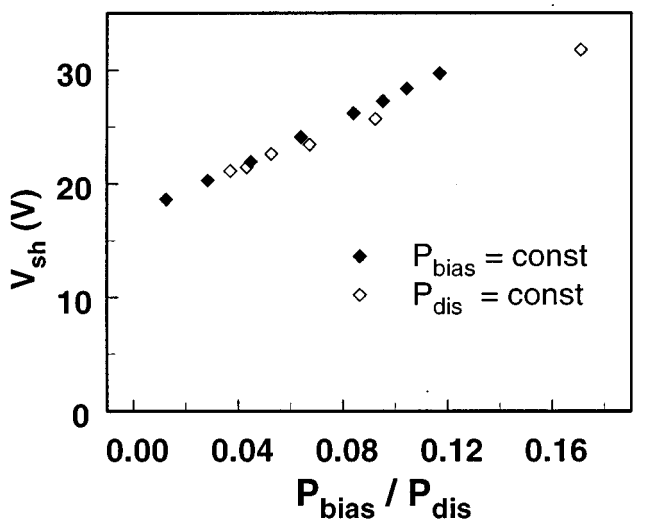

FIG. 15. The dc sheath voltage drop as a function of the ratio of bias power and plasma power, P_{bias}/P_{dis} (f_{bias} = 2.712 MHz).

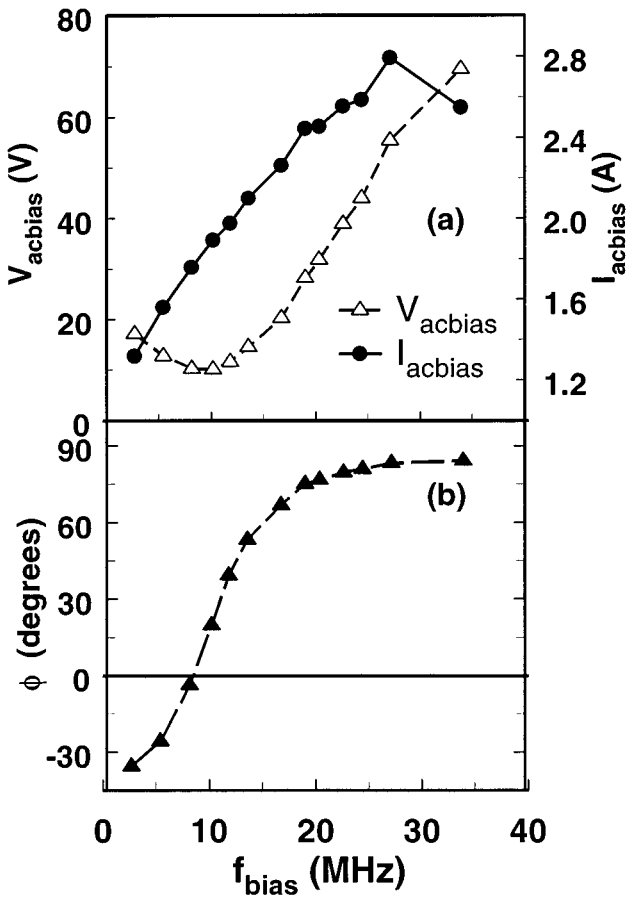

FIG. 16. (a) The fundamental component of voltage, V_{pe}, and current, I_{pe}, and (b) the phase, ϕ, between I_{pe} and V_{pe} at the surface of the biased electrode for P_{bias}=9 W.

tual loss of electrons from the plasma. As a result, the TROES signal has a minimum when there is a maximum of the current, i.e., where the electron loss is the greatest.

In the mid frequency range from 5.424 to 20.34 MHz ($f_{bias} \sim \Omega_p$), the ions become less responsive to the rf fields with increasing frequency. In the high frequency range, from 20.34 to 33.9 MHz ($f_{bias} >> \Omega_p$), the ions are essentially following only the time-averaged fields. Therefore, there is no change in the ion density as a function of time in the presheath. Consequentially, only the bulk type oscillations are seen and there is no phase shift between the bulk and presheath. The decreased signal intensities are probably related to the increased damping of ion plasma oscillations.

From combining the results of the Langmuir probe dc plasma potential measurements and the electrical measurements we conclude the following: (1) the mean ion energy cannot be controlled by changing the bias frequency, because the dc sheath voltage drop, V_{sh}, does not depend on the bias frequency [see Fig. 14(b)]; (2) the mean ion energy can be controlled by changing the ratio of bias power to plasma power, P_{bias}/P_{dis} (see Fig. 15).

Besides the mean ion energy, the shape of the IEDF is also an important parameter. As mentioned in the introduc-

tion, the IEDF for a grounded lower electrode has the relatively simple structure of a single narrow profile.[2] It is a well-known phenomenon of capacitively coupled discharges used in reactive ion etching, that the shape of the IEDF at the self-biased electrode depends on the ratio of the ion transition time across the sheath compared to the rf period.[35–37] If the ion transition time is long compared to the rf period, the ion experiences only the time-averaged sheath potential, and the IEDF has a single peak. If the ion transition time is short, the ion responds to the instantaneous sheath potential. Therefore, the IEDF will exhibit a double peak which is attributed to ions entering the sheath when the potential is at low or high energy extremes. Both of these features have been investigated by model calculations for a rf biased ICP by Hoekstra and Kushner.[3] For an ECR plasma it has been verified experimentally and theoretically by Martin and Oechsner.[38] They observed a noticeably narrower IEDF at higher bias frequencies ($f_{\text{bias}} > 16$ MHz, FWHM < 5 eV) than at lower frequencies. This indicates that a higher bias frequency may be advantageous if one is interested in a narrow IEDF. The actual measurement of the IEDF beneath a biased lower electrode and its correlation with other plasma parameters would shed some light on the possible control of the ion energy distribution. A first step in this direction is the measurement of the IEDF at the grounded chamber wall with a biased lower electrode. These measurements are in progress and will be published in a separate article.[39]

ACKNOWLEDGMENTS

The authors wish to thank M. Sobolewski (NIST) for his helpful discussions and his contribution in obtaining and analyzing the electrical probe measurements. One of the authors, (A.S.) was sponsored by a Feodor Lynen Fellowship of the Alexander von Humboldt Foundation. Another author (A.G.) was sponsored by the NIST Summer Undergraduate Research Fellowship program. This project was partially supported by the U.S. AFOSR/AOARD.

[1]J. H. Keller, Plasma Sources Sci. Technol. **5**, 166 (1996).
[2]J. R. Woodworth, M. E. Riley, D. C. Meister, B. P. Aragon, M. S. Le, and H. H. Sawin, J. Appl. Phys. **80**, 304 (1996).
[3]R. J. Hoekstra and M. J. Kushner, J. Appl. Phys. **79**, 2275 (1996).
[4]J. A. O'Neill, M. S. Barnes, and J. H. Keller, J. Appl. Phys. **73**, 1621 (1993).
[5]J. B. O. Caughman and W. M. Holber, J. Vac. Sci. Technol. A **11**, 2897 (1993).
[6]J. Hopwood, Plasma Sources Sci. Technol. **1**, 109 (1992).
[7]A. J. Perry, D. Vender, and R. W. Boswell, J. Vac. Sci. Technol. B **9**, 661 (1991).
[8]R. W. Boswell, A. J. Perry, and E. Emami, J. Vac. Sci. Technol. A **7**, 3345 (1989).
[9]J. Hopwood, Appl. Phys. Lett. **62**, 940 (1993).
[10]U. Kortshagen and M. Zethoff, Plasma Sources Sci. Technol. **4**, 541 (1995).
[11]P. Hargis Jr., K. E. Greenberg, P. A. Miller, J. B. Gerado, J. R. Torczynski, M. E. Riley, G. A. Hebner, J. R. Roberts, J. K. Olthoff, J. R. Whetstone, R. J. Van Brunt, M. A. Sobolewski, H. M. Anderson, M. P. Splichal, J. L. Mock, P. Bletzinger, A. Garscadden, R. A. Gottscho, G. Selwyn, M. Dalvie, J. E. Heidenreich, J. W. Butterbaugh, M. L. Brake, M. L. Passow, J. Pender, A. Lujan, M. E. Elta, D. B. Graves, H. H. Sawin, M. J. Kushner, J. T. Verdeyen, R. Horwath, and T. R. Turner, Rev. Sci. Instrum. **65**, 140 (1994).
[12]http://physics.nist.gov/rfcell
[13]P. Miller, G. A. Hebner, K. E. Greenberg, P. D. Pochan, and B. P. Aragon, J. Res. Natl. Inst. Stand. Technol. **100**, 427 (1995).
[14]L. J. Mahoney, A. E. Wendt, E. Barrios, C. J. Richards, and J. L. Shohet, J. Appl. Phys. **76**, 2041 (1994).
[15]A. Schwabedissen, E. C. Benck, and J. R. Roberts, Phys. Rev. E **55**, 3450 (1997).
[16]M. Sobolewski, J. Res. Natl. Inst. Stand. Technol. **100**, 341 (1995); IEEE Trans. Plasma Sci. **23**, 1006 (1995).
[17]J. R. Roberts, J. Res. Natl. Inst. Stand. Technol. **100**, 353 (1995).
[18]W. L. Wiese, M. W. Smith, and B. M. Miles, Atomic Transition Probabilities, Vol. II, Sodium through Calcium, NSRDS-NBS22 (1969), p. 193.
[19]R. E. H. Clark, J. B. Mann, G. Csanak, and A. L. Merts, Los Alamos Report LA-UR-89-2675, II, Chap. III (1989).
[20]U. Kortshagen, I. Pukropski, and M. Zethoff, J. Appl. Phys. **76**, 2041 (1994).
[21]M. A. Lieberman and A. J. Lichtenberg, *Principles of Plasma Discharges and Materials Processing* (Wiley, New York, 1994).
[22]P. A. Chatterton, J. A. Rees, N. L. Wu, and K. Al-Assadi, Vacuum **42**, 489 (1991).
[23]V. A. Godyak, R. B. Piejak, and B. M. Alexandrovich, Plasma Sources Sci. Technol. **1**, 36 (1992).
[24]V. A. Godyak and N. Sternberg, Phys. Rev. A **42**, 2299 (1990).
[25]U. Flender, B. H. Nguyen Thi, and K. Wiesemann, Plasma Sources Sci. Technol. **5**, 61 (1996).
[26]B. P. Wood, M. A. Lieberman, and A. J. Lichtenberg, IEEE Trans. Plasma Sci. **23**, 89 (1995).
[27]K.-U. Riemann, J. Phys. D **24**, 493 (1991).
[28]M. M. Turner, Phys. Rev. Lett. **71**, 1844 (1993).
[29]V. A. Godyak, R. B. Piejak, and B. M. Alexandrovich, Plasma Sources Sci. Technol. **3**, 169 (1994).
[30]J. Hopwood, C. R. Guarnieri, S. J. Whitehair, and J. J. Cuomo, J. Vac. Sci. Technol. A **11**, 147 (1993).
[31]M. Malingre, Radio Sci. **19**, 400 (1984).
[32]G. A. Hebner, J. Appl. Phys. **80**, 2624 (1996).
[33]G. M. Sessler, Phys. Lett. **22**, 363 (1966).
[34]S. Watanabe and H. Tanaca, Plasma Phys. **15**, 501 (1970).
[35]A. D. Kuypers and H. J. Hopman, J. Appl. Phys. **67**, 1235 (1990).
[36]J. Liu, G. L. Huppert, and H. H. Sawin, J. Appl. Phys. **68**, 3916 (1990).
[37]A. Manenschijn and W. J. Goedheer, J. Appl. Phys. **69**, 2923 (1991).
[38]D. Martin and H. Oechsner, Vacuum **47**, 1017 (1996).
[39]M. Sobolewski and Y. Wang (unpublished).